Preparation of mesoporous γ-Al₂O₃ with high surface area from an AlOOH extract of recycling biomass ash

Mauricio Gómez[a], Jaime Pizarro[a], Ximena Castillo[a], Carlos Díaz[a], Alessio Ghisolfi[b], María de Lourdes Chávez[c], Diego Cazorla-Amorós[b], Jesús Arenas-Alatorre[d]

a Departamento de Ingeniería Geográfica, Facultad de Ingeniería, Universidad de Santiago de Chile, Santiago, Chile

b Instituto Universitario de Materiales, Departamento de Química Inorgánica, Universidad de Alicante, Apartado 99, 03080, Alicante, España

c Departamento de Químicas Inorgánica y Nuclear, Universidad Nacional Autónoma de México

d Instituto de Física, Universidad Nacional Autónoma de México, México D.F., México

ABSTRACT

This study explores the potential application of recycled materials extracted from arboreal ABA (ABA); this waste is used as an alternative source of aluminium oxyhydroxide for the synthesis of γ-Al₂O₃ with high surface area-based mesoporous materials with interesting applications in environmental remediation. The aluminium present in ABA was extracted by desilication and reflux in acid and subsequently converted to mesoporous γ-Al₂O₃ via a sol-gel process with Pluronic P-123 as surfactant. The surface of that material was successfully functionalized with racemic glycine (GLY) and N,N-dimethylacetamide (DMAC) by liquid impregnation in order to study and compare their applications in capture of Fe^{3+} cations. All the materials were unambiguously characterized by adsorption-desorption isotherms of N_2 at 77 K, X-ray fluorescence (XRF), elemental analysis (EA), X-ray diffraction (XRD), diffuse reflectance infrared fourier transform spectroscopy (DRIFTS), scanning electron microscopy with dispersive energy detector of X-ray (SEM-EDS), transmission electronic microscopy (TEM) and X-ray photoelectron spectroscopy (XPS). This process afforded γ-Al₂O₃ with high purity and the surface area of the mesoporous materials ranged from 115 $m^2\ g^{-1}$ for AlOOH to 230 $m^2\ g^{-1}$ for γ-Al₂O₃. The achieved surface functionalization was of 2 and 3 wt% with glycine and DMAC, respectively. The effective performance of these materials (both pristine and functionalized) in the removal of Fe^{3+} ions from an aqueous solution was evaluated in batch systems. In particular, the materials presented extraction capacities of about 78.2% for bare γ-Al₂O₃, 83.2% for Al-GLY and 93.9% for Al-DMAC.

Keywords: Biomass ash recycling, alumina extraction, mesoporous γ-Al₂O₃, functionalization, iron adsorption.

1. Introduction

In the past decade, mesostructured materials have been applied across diverse scientific fields including processes such as heterosedeneous catalysis, environmental remediation as degradation of HCHO to CO_2 and H_2O, CO oxidation, and dye and metal adsorption (Fe^{3+}, Cu^{2+}, Zn^{2+}, Pb^{2+}) [1–5]. Such materials present high surface areas and interesting surface chemical versatility that allows them to be functionalized with organic molecules; thus, improving their catalytic and adsorbent properties [6]. After the first development of mesoporous structures, named as the M41S family [7], other mesostructured materials were prepared using copolymers of three non-ionic blocks of the type EOnPOmEOn as surfactants and, generally, were named SBA [8]. Both the M41S and the SBA were obtained using silica as a precursor and the next step was to replace silica with other precursors such as Al_2O_3, Fe_2O_3, TiO_2, ZrO_2 and mixed oxides to obtain new mesoporous material [9–11].

Since 1998, multiple advances in the synthesis of mesoporous materials have been achieved, with the development of new pore structures and synthetic routes as well as through the use of different structure precursors and types of surfactants. These developments also included the functionalization of the mesoporous surface, thus extending the advantages of mesostructures to multiple applications [12,13]. An interesting functionalization of mesoporous materials consists of decorating the inorganic structure of the pristine materials with functional, chemically active, organic molecules, with the aim of combining the functional variety of organic chemistry with the thermal stability of inorganic substrates [14].

The process of surface functionalization of metal oxides starts by a hydrolysis reaction to generate metal alkoxides, which can be used as tethering points for suitable organic molecules. These products can be achieved by two routes. The first one is a post-synthetic functionalization, where the surface modification takes place after the formation of the mesoporous structure. The second route consists of the simultaneous condensation of the alkoxide in the presence of the organic precursor, in a 'co-condensation' process [15]. Mesoporous alumina is a low-cost, non-toxic material that has uniform pores and high surface area with a narrow pore size distribution [11]. Mesoporous alumina has been used as anionic colorant adsorbent with outstanding results [16–21], CO_2 and fluorine adsorption [22,23] and removal of metal species such as Cr, As, Fe, Cu, Cd and Pb [24,25]. The adsorption of Fe^{3+} on mesoporous material was studied to contribute to the development of a purification technology for this metal that facilitates the efficient use of

67 recirculation water in the pulp industry [26].

68   Worldwide, intense industrial activity generates vast amounts of waste every year. The
69 treatment and disposal of these wastes generate several challenges and concerns. Therefore, waste
70 management has become a highly profitable way of transforming, valuing and reusing these by-
71 products, especially from the circular economy perspective, wherein pollutant emissions are shifted
72 by reuse and recycling [27,28]. In 2040, the total global generation of electricity from coal will be
73 73% higher than in 2010 [28], which entails improving the conventional methods of disposal of fly
74 ash wastes that until now are mainly based on their use as additives for construction materials and
75 landfills [29]. Another application for the recycling and reuse of fly ash wastes is pelletization for
76 further use as soil fertilisers, or for acid/basic extraction of heavy metals, in order to reduce the
77 environmental impact of the industrial activity and to seek additional economic value from such
78 wastes [30–32]. An alternative application for fly ash is as a cheap source of alumina, thus reusing
79 the residual product from the combustion of coal and wood or from different industrial activities
80 [33]. The use of fly ash in the synthesis of mesoporous structures of the type MCM-41 and SBA-
81 15 [34–36] created materials of high structural stability and good periodicity on the porous
82 structure. Nevertheless, the use of fly ash aluminium oxyhydroxide extracts as precursors of
83 mesoporous structure has not yet been well-studied.

84   This work deals with the recycling of arboreal biomass ash (ABA) as a source of aluminium
85 oxyhydroxide, as precursors for the preparation of γ-Al_2O_3-based mesoporous structures with high
86 surface area. The main contributions of this study are the recycling of a waste as an alternative
87 source of new adsorbent materials for application in environmental remediation. The γ-Al_2O_3
88 materials obtained were then functionalized with N,N-dimethylacetamide (Al-DMAC) and
89 Glycine (Al-GLY) in order to enhance their Fe^{3+} adsorption capacity. The method developed in
90 this work is proposed for further applications in wastewater treatments because this metal is a
91 typical industrial water pollutant that produces taste, colour and odour alterations in natural
92 effluents [37,38]. The arboreal biomass ash (ABA), the aluminium extraction (AlOOH) and the
93 synthesized aluminium mesoporous matrix (γ-Al_2O_3) were well characterized by XRF, XRD,
94 SEM, TEM, adsorption-desorption isotherms, DRIFTS and XPS analysis and compared with the
95 γ-Al_2O_3 functionalized with N,N-dimethylacetamide (Al-DMAC) and glycine (Al-GLY). Their
96 Fe^{3+} adsorption capacity was also analysed.

97

2. Materials and methods

2.1. Aluminium extraction from arboreal biomass ash (ABA)

The ABA used was obtained from a local pulp mill, located in the Biobío region, Chile. In the combustion process, this industry uses Radiata Pine and Eucalyptus trees; therefore, the ABA is a mix of these. For the aluminium extraction method, two stages took place [39]; the first process was the desilication of the performed using a 1:1:1 mixture of ABA, NaOH and $NaHCO_3$ (the original method used Na_2CO_3, we changed it to $NaHCO_3$ in order to reduce the amount of sodium remaining, which could interfere with the final purity of the synthesized material). In an agate mortar, the reactants were mixed and ground with drops of water to facilitate mixing. Eventually, the mixture was dried at 60°C for 24 h to allow the water to evaporate, and then it was calcined at 700°C for 2 h. The second stage consisted of refluxing 1 gram of the calcined products in 5 mL of concentrated HCl (10.5 M) for 2 hours to solubilize the aluminium. During this process, sodium silicates are formed which then form a stable, non-soluble phase as mentioned in the reference [39]. Once the reflux was concluded, the supernatant was filtered. The obtained filtrate was treated with NaOH 40 wt% to promote the precipitation of the cation and to minimize impurities; the solids were separated from the solution by filtering. Finally, the pH of the supernatant was adjusted to pH 7 (6 M HCl) to precipitate the aluminium oxyhydroxide. The solid obtained was amorphous aluminium oxyhydroxide of the kind AlOOH.

2.2. Mesoporous material synthesis

The synthesis started by dissolving 1.0 g of Pluronic P-123 in 20.0 mL of ethanol at room temperature. Afterwards, 1.5 mL of nitric acid 67 wt% and 2.04 g of AlOOH extracted from ABA were added, and stirred at room temperature for 5 h, then it was dried at 60°C for 48 h. Finally, the surfactant Pluronic P-123 was removed by calcination at 550°C for 5 h. The resulting product mesoporous γ-Al_2O_3 was then placed in storage for further characterization. It is well known that γ-Al_2O_3 may be obtained by calcination of aluminium oxyhydroxide in a range of 400°C to 900°C [22,24] where no surfactants are required; nevertheless, these methods produced γ-Al_2O_3 with 300 m^2 g^{-1} to 400 m^2 g^{-1} surface area, presenting several disadvantages in the final product, such as pore size distribution, and surface area control. In order to address these problems, surfactant P-123 has been used [8,22–24,40].

129

2.3. Functionalization of γ-Al_2O_3

The functionalization of the material with N,N-dimethylacetamide (Al-DMAC) and glycine (Al-GLY) was based on the method developed in our previous work, by mixing and refluxing the γ-Al_2O_3 precursors and the functionalizing group for 12 h [36]. This procedure remains the same for both syntheses.

2.4. Physicochemical and morphological characterization

Morphological characterization of porous materials was performed using transmission electron microscopy (TEM) (JEOL JEM-2010 Plus); the microstructural morphology and chemical composition were performed by scanning electron microscopy (SEM-EDS) (JEOL JSM-5900-LV ESEM and Oxford ISIS brand X-ray energy dispersive spectroscopic microanalyzer EDS); the characterization of phases was performed by X-ray powder diffraction (XRD) on a Siemens D500 diffractometer, with CuKα radiation filtered with Ni, at 1.5406 and 1.54184 Å, a time constant of 3 s and an angular step speed of 2° per min from 5 to 80° of 2θ. The elemental analysis and the purity estimation of the precursor and the synthesized structure were carried out by X-ray fluorescence (XRF) (Philips Magix Pro model PW2400, equipped with the SuperQ analytical software). CHNS elemental analyses were performed with an elemental microanalyzer (Micro TruSpec, LECO); the study of functionalization capacity of the mesoporous structure, γ-Al_2O_3, with DMAC and GLY and capture of Fe^{3+} performed by X-ray photoelectron spectroscopy (XPS) (VG-Microtech Multilab 3000 device equipped with a hemispherical electron analyzer with 9 channeltrons with step energy of (2-200 eV) and an X-ray radiation source with Mg and Al anodes). The energy range studied was from 100 to 4000 eV with emphasis on binding energies at 390-400 eV (N 1s) and 700-740 eV (Fe 2p). Determination of functional groups on the surface of the mesoporous structure was done by diffuse reflectance infrared fourier transform spectroscopy (DRIFTS) (FTIR JASCO 4100) in the KM mode from 400 to 4000 cm^{-1}. Nitrogen adsorption-desorption isotherms were performed at 77 K using an Autosorb-6B (Quantachrome) gas analyser; total pore volume was determined at p/p$_0$= 0.99, average pore size was determined from the BJH method and the surface area was measured using the BET method, both values were estimated with Quantachrome software.

159

160 2.5. Preliminary Fe^{3+} Adsorption Tests

161 The Fe^{3+} capture tests were performed in batch systems following the same process [36]. The Fe^{3+}

162 solutions were prepared from a standard solution of 1000 ppm of $Fe(NO_3)_3$ (Merck) and

163 conditioned to pH 2.0, 2.5 and 3.0. The pH was controlled along the test with HNO_3, 0,1 M, and

164 with NaOH, 0.1 M. The percentage of Fe^{3+} ion removal ($\%R_{Fe^{3+}}$) and the equilibrium adsorption

165 amount of Fe^{3+} q_e (mg g^{-1}) were calculated using equations 1 and 2:

166

167 $$\%R_{Fe^{3+}} = \frac{C_0 - C_e}{C_0} * 100 \qquad (1)$$

168

169 Adsorption amount of Fe^{3+} per gram (g) of adsorbent (mg g^{-1}) is

170

171 $$q_e = \frac{(C_0 - C_e) * V}{W} \qquad (2)$$

172

173 Where C_0 is the initial adsorbate concentration in the solution (mg L^{-1}), C_e is the

174 concentration of adsorbate in the solution at equilibrium (mg L^{-1}), V is the volume of the

175 solution (mL), and W is the mass of adsorbent (g).

176

177

178 **3. Results and Discussion**

179

180 3.1. Materials characterization

181 ABA was characterized by XRF elemental analysis (Table 1). The chemical composition of ABA

182 shows that silica has a larger presence compared to all other elements. In supplementary materials

183 (S1) shows the XRD pattern of ABA, which confirms that the present phases are: (Q) SiO_2 quartz,

184 (Al) Al_2O_3, (M) $Al_6Si_2O_{13}$, Mullite, (Fe) Fe_2O_3 and (B) Al(OOH). The phases detected are

185 polycrystalline, which is expected since the temperature at which ABA are obtained hinders the

186 presence of amorphous phases [36]. The adsorption-desorption isotherm of N_2 at 77 K for ABA is

187 of type IV with a H3 hysteresis cycle [41] (see supplementary materials S2). This isotherm and

188 hysteresis indicated a solid characterized by a low porosity, a consequence of the interparticle

189   porous formation along with low pore volume and surface area. The porous texture parameters

190   obtained can be seen in Table 2 by the predictive methods BET and BJH. More information about

191   chemical composition and structure of ABA can be found in this reference [36]. This

192   characterization makes it possible to estimate a SiO_2/Al_2O_3 ratio in ABA of 2.4, an optimal value

193   for the extraction of alumina [33,35], the surface area and porosity of ABA, 18 m^2 g^{-1} and 3.8 nm,

194   respectively, which contributes to this process, giving extra reactivity to the Alumina extraction.

195

196   3.2. Extraction AlOOH and synthesis of mesoporous γ-Al_2O_3

197   The alumina was extracted from ABA by a desilication method and subsequent acid treatment,

198   resulting in a solid amorphous aluminium oxyhydroxide of the type AlOOH, the ABA contained

199   19.5 wt% Al_2O_3, see Table 1; the extraction process yields 90% aluminum (AlOOH). Fig. 1a shows

200   the XRD pattern of the obtained aluminium oxyhydroxide, the reflection peaks and the registered

201   angles confirm the presence of amorphous aluminium oxyhydroxide (AlOOH). AlOOH is obtained

202   at room temperature and under aqueous conditions, which generates a crystalline structure distorted

203   by the OH groups resulting in an amorphous pseudoboehmite-type AlOOH [42]. It can be observed

204   that there are no additional signals belonging to the pristine phases of the ABA; thus, the precursor

205   used for the synthesis of γ-Al_2O_3 is in agreement with that previously reported [42]. Once the

206   AlOOH is transformed into mesoporous γ-Al_2O_3 by the sol-gel synthesis method, it is observed

207   that the γ-Al_2O_3 obtained has mainly an amorphous character without residual traces of the

208   presence of the starting product AlOOH (Fig. 1b). This is expected because the surfactant

209   extraction took place at 550°C, temperatures at which crystallization of the γ-Al_2O_3 does not take

210   place. In fact, crystallization occurs at temperatures above 750°C with a substantial loss of surface

211   area [43,44]. XRD patterns demonstrated the crystalline phase change from AlOOH to γ-Al_2O_3

212   produced by surfactant P-123 and calcination at 550°C; the crystallinity of the γ-Al_2O_3 is

213   responsible for the active sites, pore size and accessibility of adsorbates on the surface.

214   The DRIFTS spectrum for AlOOH (supplementary materials S3a) shows the presence of O-

215   H broad band between 3700 cm^{-1} and 3000 cm^{-1}; thus, flection bands at 1634 cm^{-1}, 1502 cm^{-1} and

216   1410 cm^{-1} from OH groups linked to Al were observed, forming the bond Al-O-H, confirmed with

217   1150 cm^{-1} and 1022 cm^{-1} bands, which are typical of boehmite. At approximately 900 cm^{-1}, a

218   deformation band of the surface groups Al-OH appeared. Finally, at 529 cm^{-1}, a flection band in

219   the plane of the angle HO-Al=O [45] appeared, which confirmed that the present functional group

220   in the extracted structures from ABA is AlOOH. Likewise, the DRIFTS spectrum for γ-alumina

221   (supporting information S3b) showed a decrease in intensity of the bands O-H between 3700-3000

222   cm^{-1}. In addition, the Al-O-H bands were appreciated at 1634 cm^{-1}, 1502 cm^{-1}, 1410 cm^{-1}, 1150

223   cm^{-1} and 1022 cm^{-1}. The disappearance of bands at 900 cm^{-1} and 529 cm^{-1} demonstrated the

224   structural change suffered by AlOOH when it was transformed into γ-alumina [45]. The presence

225   of Pluronic P-123 was not detected by DRIFTS analysis, suggesting that the surfactant calcination

226   was quantitative.

227   The XRF analyses were performed to AlOOH and γ-Al_2O_3, Table 1 shows the results; in both

228   cases purity exceeded 90%. SEM micrographs and TEM images of ABA, AlOOH and γ- Al_2O_3 are

229   shown in Figs. 2 and 3. The SEM images for ABAs (Fig. 2a and 2b) show that the materials are

230   constituted by a mixture of spherical particles and agglomerates of non-defined shape. No apparent

231   porosity is observed on the surface of the particles by TEM (Fig. 3a and 3b) and interparticle spaces

232   formed by particle agglomeration provided the material with a certain porosity. This latter

233   observation agrees with the N_2 adsorption-desorption isotherm at 77 K (S2). Therefore, the starting

234   material is a highly heterogeneous material, both in its chemical composition and in its crystalline

235   and morphological structure. On the other hand, for AlOOH and γ- Al_2O_3, an apparent porosity

236   was observed in both cases. Fig. 2c shows an apparent flat surface for AlOOH. However, higher

237   magnification (Fig. 2d) shows the presence of particle agglomerates of AlOOH, without a defined

238   structure and with a heterogeneous distribution of pores. Synthesised γ-Al_2O_3 (Fig. 2e and 2f)

239   presents an irregular surface with higher apparent porosity, homogeneity and uniformity than the

240   AlOOH extracted. These differences between AlOOH and γ-Al_2O_3 are also observed by TEM

241   micrographs (Fig. 3), where both the porosity and the morphology of the γ-Al_2O_3 (Fig. 3e and 3f)

242   particles are more homogeneous and consistent than those of AlOOH (Fig. 3c and 3d).

243   Fig. 3f clearly shows the effect of the surfactant P-123 in the γ-Al_2O_3 porous structure.

244   Surfactant P-123 apparently produces a spherical porosity morphology due to the distortion or low

245   definition in the formation of hexagonal pores, suggesting the possible existence of a worm-like

246   structure, possibly associated with the use of the AlOOH extract and not a synthetic aluminium

247   compound [43,45]. Due to the low crystallinity of the samples, there were no images obtained from

248   the dark field for both samples. Complementary to the XRF analysis, the EDS analysis was

249   performed. The results obtained are collected in supplementary materials S8. EDS analysis shows

250   the presence of Cl^- in the structure AlOOH, in agreement with the XRF results in Table 1. Cl^- came

251   from HCl used during the aluminium extraction stage which was not removed completely along

252   the extraction product washing stage. In contrast, the analysis for γ-Al$_2$O$_3$ did not show the presence

253   of Cl$^-$ because, during the synthesis of the γ-Al$_2$O$_3$ mesoporous matrix, the AlOOH used as

254   precursor was diluted in ethanol and nitric acid, in which residual Cl$^-$ was eliminated from the

255   mesoporous matrix during the synthesis process. It is known that, during the synthesis of SBA-15

256   type materials, both HCl and/or HNO$_3$ [40,46,47] are used as structure catalysts to favour the

257   surfactant-precursor interaction. The use of AlCl$_3$ [48] as precursor is also known and residual Cl$^-$

258   elimination occurs during the γ-Al$_2$O$_3$ synthesis process.

259   The adsorption-desorption isotherms of N$_2$ at 77 K of AlOOH (Fig. 4a) and of γ-Al$_2$O$_3$ with

260   broad hysteresis cycles (Fig. 4b) are of the type IV, characteristic of mesoporous solids. In the case

261   of AlOOH, there was no presence of a plateau at high relative pressures, indicating a type H3 cycle

262   [42]; this is expected for particles forming slit-shaped porous agglomerates. In the case of γ-Al$_2$O$_3$,

263   its hysteresis cycle presented a plateau at high relative pressures during the desorption branch.

264   Besides, it was observed that the adsorption-desorption branches in the high relative pressure

265   regions are parallel, typical of the H1 cycle. The PSD graph (S4) confirms the mesoporosity and

266   narrow porosity observed in the isotherms obtained [41]. These cycles have been observed in

267   mesoporous materials with narrow pore size distribution, with cylindrical pores, or spherical

268   particle agglomerates with uniform sizes and distributions. In γ-Al$_2$O$_3$, porosity was not a result of

269   spherical agglomerates, a fact that was evidenced by the SEM and TEM micrographs (Fig. 2e-f

270   and Fig. 3e-f), which suggested a worm-like structure, confirming the templating effects of

271   surfactant on porous structure. In summary, the hysteresis loop (Fig. 4) close to the higher relative

272   pressure p/p$_0$ of 0.7 indicates the larger pore size of the sample with cylindrical pores, and the H1

273   isotherm obtained indicates narrow porosity, uniform pore size distributions and cylindrical pore

274   morphology, confirming the morphology shown in Fig. 3c.

275   The obtained surface areas, both for AlOOH and γ-Al$_2$O$_3$, were 115 m^{2}g^{-1} and 300 m^{2}g^{-1}

276   (Table 2), respectively. It is possible to observe that these values are higher than those reported

277   [22], which is attributed to the fact that in previous studies [22] the P-123 surfactant was not

278   eliminated. Also, Fig. 4 shows that adsorption capacity increased from 160 cm^3 (STP) g^{-1} to 600

279   cm^3 (STP) g^{-1}, which indicates that the AlOOH surface properties were enhanced when transformed

280   into γ-Al$_2$O$_3$, as expected. The results for the effect of sol-gel synthesis and heat treatment were

281   consistent with much larger average pore size distribution than found in [40] (BET surface area of

282   300 m^2 g^{-1} and a pore volume of 0.95 cm^3 g^{-1}). The large surface areas, narrow pore size

283   distributions and good accessibility of mesoporous combined with excellent thermal stability

284   promised potential applications of these mesoporous γ-Al_2O_3 in adsorption and functionalization

285   process.

286

287   3.3. Functionalization of mesoporous γ-Al_2O_3.

288   S5 and S6 in supplementary materials depict the proposed reaction mechanisms for the

289   functionalization of synthesized mesoporous γ-Al_2O_3 with N,N-dimethylacetamide (Al-DMAC)

290   and γ-Al_2O_3 with Glycine (Al-GLY). The first proposed mechanism (S5) shows the effect that

291   aluminium ions have on DMAC carboxylates. The aluminium hydroxyl species react with the

292   carbon atom of the amide group of DMAC forming a new Al-O-C bond between DMAC and γ-

293   Al_2O_3. Fig. 5a includes the DRIFTS spectrum of functionalized γ-alumina with N,N-

294   dimethylacetamide (Al-DMAC). A broad band was observed in the interval from 3700 cm^{-1}- 3000

295   cm^{-1}. This signal corresponds to the O-H group formed by the protonation of the DMAC carbonyl

296   group. The DRIFTS spectrum also shows bands at 1580 cm^{-1}, 1470 cm^{-1} and 1420 cm^{-1}, typical of

297   the presence of C-N and C-C bonds and CH_3 groups of tertiary amides. It is also noteworthy that

298   there is absence of a band close to 1700 cm^{-1} that confirms the modification of the carbonyl group

299   due to the reaction with the hydroxyl groups of the γ-Al_2O_3. The band at 1340 cm^{-1} is related to the

300   methyl group of N,N-dimethylacetamide. Finally, the bands between 900 cm^{-1} and 1100 cm^{-1} were

301   associated with the presence of O-C-N and O-C-O of DMAC bonds grafted to the mesoporous γ-

302   Al_2O_3 structure [49,50].

303   S6 shows the proposed mechanism of functionalization of γ-Al_2O_3 with glycine (Al-GLY).

304   In this mechanism, a peptide bond is shown by the union of GLY-GLY and the ester formed by the

305   union γ-Al_2O_3–GLY, due to the zwitterionic character of glycine [50–53]. The DRIFTS spectrum

306   of Fig. 5b presents a series of bands between 3600-3000 cm^{-1}. These bands indicated the presence

307   of primary, secondary amines and hydroxyl groups. The presence of bands at 1642 cm^{-1} and 1520

308   cm^{-1} revealed a GLY-GLY bond, a peptide bond expected in glycine since it is an amino acid that

309   can exist in the zwitterion form. The splitting of signals located between 1400 cm^{-1} and 1300 cm^{-1}

310   (O=C-O-R), and the interval between 1200 cm^{-1} (O=C-NH-R) and 900 cm^{-1} (O=C-O-Al)

311   confirmed the formation of peptide bonds GLY-GLY (O=C-NH-R) and γ-Al_2O_3-GLY by means

312   of esterification of GLY carboxyl acid and the hydroxyl species at the surface of the hydrated γ-

313   Al_2O_3 (O=C-O-Al) [51–53]. Previous studies carried out on the zwitterion behavior of the GLY

314   moiety of the Al-GLY or Si-GLY material surfaces, demonstrate the strong dependence on pH and

315   functionalization temperature [51–53]. Thus, the GLY-GLY bond would be formed between pH 2

316   to 9, being the ideal 6 at a temperature of up to 160°C; at higher temperatures, GLY would form

317   the cyclic dimer diketopiperazine (DKP). In both cases, the Gly-Gly bond is observed in the 1300-

318   1800 cm^{-1} region analogous to the band of NH_3^+ or ^+H_3N-CH_2-COO- ions, which was not observed

319   in the case of the non-zwitterion GLY (-NH_2 neutral) or in DKP (=N-H) [51]. So, it can be said

320   that the mechanism proposed in S6 is a consistent empirical and theoretical approximation. The

321   amount of N groups functionalized with γ-Al_2O_3 have been estimated from CHN analysis: 0.63

322   mmol g^{-1} of N in Al-DMAC, 0.29 mmol g^{-1} of N in Al-GLY and no presence of N in γ-Al_2O_3,

323   confirming successful functionalization. Furthermore, it is observed that the C:N ratio of DMAC

324   is 3:1 and in glycine 2:1 (Supplementary Table S7), demonstrating that there is no decomposition

325   of the organic structure; this result contributes to justification of the proposed functionalization

326   mechanism.

327

328   3.4. Adsorption characterization of Fe^{3+} and environmental factor (E-factor).

329   The functionalization of the γ-Al_2O_3 matrices aims to improve the adsorption of Fe^{3+} and thus

330   produces higher affinity of the mesoporous matrix against this adsorbate due to N-Fe interactions.

331   Mesoporous matrices are not selective by themselves [36], so functionalizing them is a good option

332   to provide the selectivity that these matrices lack. The increase of the number of active sites allows

333   higher Fe^{3+}capture capacity. Functionalized γ-Al_2O_3 matrices have a higher adsorption capacity

334   than non-functionalized γ-Al_2O_3 matrices (78% pure γ-Al_2O_3 <83% Al-GLY <94% Al-DMAC).

335   This greater capture capacity is the result of the groups that contain N (Table S7). For the

336   functionalization process, being a surface process where organic molecules with specific functional

337   groups are grafted to the surface of the mesoporous material, it is necessary to use techniques that

338   provide information about the process that generated the functionalization. XPS allows us to

339   analyze interactions and environments of atoms and molecules that form analyzed structures; so,

340   this technique allowed us to study and formulate a functionalization mechanism [36], which was

341   complemented with DRIFT, which was already discussed. S5 and S6 show the proposed

342   mechanisms for functionalization with DMAC and GLY. In addition, possible Fe^{3+} interactions

343   with the functionalized matrices were evaluated with XPS, where it was identified that the amine

344 groups are suitable for increasing the adsorption capacity and selectivity of Fe^{3+}. Fig. 6 contains

345 the results of the XPS analysis. The spectra are presented to compare the γ-Al_2O_3 before (Fig. 6a

346 and 6b) and after the functionalization (Fig. 6c and 6d). The N 1s and Fe 2p spectra for the

347 mesoporous γ-Al_2O_3 (Fig. 6a and 6b) show that there is not any presence of nitrogen nor iron on

348 the non-functionalized γ-Al_2O_3. Fig. 6c (γ-Al_2O_3-DMAC) and 6d (γ-Al_2O_3-GLY) contain the N 1s

349 spectra for the functionalized materials, which confirm the presence of nitrogenated species in the

350 functionalized γ-Al_2O_3 [54], both with DMAC and GLY [52,55]. From the previous study, it was

351 demonstrated that γ-Al_2O_3 is a good candidate for surface functionalization and can even be used

352 as a support structure for the preparation of heterogeneous catalysts, because of their high surface

353 area, pore volume and pore size.

354   Table 3 contains the results obtained in the adsorption of Fe^{3+} in q_e (mg g^{-1}) and in adsorption

355 percentage. The adsorption in the three matrices at pH 2.0 and 2.5 was between 11 and 14 mg g^{-1}

356 of material with approximately 50% of Fe^{3+} adsorption. In this pH interval there was a strong

357 competition between H^+ and Fe^{3+} species for the active sites in the matrices, a fact that would

358 explain the low removal percentage. At pH 3.0, the Fe^{3+} removal is 78.2% in the non-functionalized

359 matrix, 83.21% in the functionalized matrix Al-GLY and at 93.88% at Al-DMAC. This increase

360 in the Fe^{3+} removal capacity can be explained by the higher affinity of active sites in the matrices

361 for Fe^{3+} than H^+. Fig. 7 shows the q_e (mg g^{-1}) curves versus pH for the three matrices studied.

362   For the present study of adsorption, it is important to mention the high capacity of γ- Al_2O_3

363 without being functionalized, which achieved about 80% capture of Fe^{3+}, proving it to be a good

364 adsorbent material. Table 4 shows the results of the literature reviews [56–60], where it can be

365 observed that the matrices synthesized and functionalized in this project are comparable with

366 different modified adsorbent materials. In order to study the interaction between the Fe species and

367 the matrices, XPS analyses of the functionalized matrixes after Fe adsorption were performed. The

368 XPS spectra of N 1s are shown in Fig. 8a (Al-DMAC) and Fig. 8b (Al-GLY), respectively. These

369 spectra show the presence of a new N 1s band with respect to that observed in Fig. 6. Such a band

370 was located at 407 eV approximately, which indicated that the adsorbed Fe^{3+} ions are electrically

371 compensated by the NO_3^- ions [54]; this electrical compensation comes from the preparation of

372 Fe^{3+} solutions (see section 2.4). In addition, a distortion of the N 1S band at 401 eV is observed

373 (Fig 8), suggesting that the Fe adsorption-functionalized matrix interactions would be occurring by

374 the action of the electronic pair available on the amine nitrogen of the functionalizing molecules

375 [29,31,36].

376   The XPS spectra for Fe 2p, included in Fig. 8c and Fig. 8d, clearly show the presence of the

377 Fe species adsorbed on the functionalized materials. In both cases, the presence of bands at 711 eV

378 and 724 eV belonging to Fe^{3+}, with their respective satellite bands at 719 eV and 733 eV, indicates

379 that iron is captured by the mesoporous matrix whilst it did not suffer alterations from the initial

380 oxidation state [61–63]. The XPS results suggest an electrostatic interaction between N-Fe present

381 in both DMAC and GLY, combined processes of physisorption and chemisorption are not ruled

382 out.

383   E-factor was evaluated to estimate the sustainability and environmental impact of the

384 synthesis process of the functionalized mesoporous material; this was calculated according to

385 equation 3:

386

387   E-factor = (17.1g extraction 1) + (52.3 g SiO_2) + (53.2 extraction 2) + (2.3 g red mud) +

388   (8.41 g synthesized nanomaterial)/0.45 g functionalized material = 296.4.   (3)

389

390

391 The value of the E-factor is in a low range compared to the values reported for the synthesis of

392 nanomaterials, a result that allows estimating that the process of obtaining this nanomaterial has a

393 low environmental impact [64].

394

395 **4. Conclusion**

396 This study deals with the recycling of a waste, tree ABA, as an alternative source to conventional

397 aluminium to synthesize mesoporous materials with high surface area. The extracted aluminium

398 by desilication and acid reflux was amorphous aluminium oxyhydroxide of the type AlOOH, and

399 it was used as a precursor for the preparation of mesoporous γ-Al_2O_3 structures. Such modification

400 on the aluminium structure resulted in an increase of the surface area from 115 m^2g^{-1} to 230 m^2g^{-1}.

401 TEM analysis and adsorption-desorption isotherms of N_2 at 77 K suggested a worm-like particle

402 configuration, with spherical porous canals in γ-Al_2O_3. This structure is created by the use of

403 Pluronic P-123 surfactant as a template. Furthermore, with the aim of improving and comparing

404 adsorption ability to γ-Al_2O_3, the surface of the pores was functionalized with DMAC and GLY,

405 with a post-synthesis liquid impregnation. Such derivatization resulted in an increased capacity of

406   Fe^{3+} adsorption in aqueous phase: from 78.2% in the non-functionalized matrix to 83.21% in the

407   functionalized matrix Al-GLY and 93.88% for Al-DMAC, whose E-factor is 296.4. These results

408   proved that γ-Al_2O_3 behaves as an excellent adsorbent material for metal ions and that, by

409   modifying its surface, it is possible to increase its performance and possibly tailor its affinity toward

410   particular target species. From this study, we could conclude that γ-Al_2O_3 synthesized from an

411   extract of AlOOH from ABA is a good candidate to be used as a water remediator or as a support

412   for heterogeneous catalysts, due to its high surface area, pore volume, pore size and easy tunability

413   via surface modifications.

414

426

427   **References**

428   [1]   A. Walcarius, L. Mercier, Mesoporous organosilica adsorbents: Nanoengineered materials

429   for removal of organic and inorganic pollutants, J. Mater. Chem. 20 (2010) 4478–4511.

430   https://doi.org/10.1039/b924316j.

431   [2]   F. Collins, A. Rozhkovskaya, J.G. Outram, G.J. Millar, A critical review of waste resources,

432   synthesis, and applications for Zeolite LTA, Microporous Mesoporous Mater. 291 (2020)

433   109667. https://doi.org/10.1016/j.micromeso.2019.109667.

434   [3]   J. Čejka, R. Millini, M. Opanasenko, D.P. Serrano, W.J. Roth, Advances and challenges in

435   zeolite synthesis and catalysis, Catal. Today. 345 (2020) 2–13.

436   https://doi.org/10.1016/j.cattod.2019.10.021.

437   [4]   Y.R. Lee, J.T. Soe, S. Zhang, J.W. Ahn, M.B. Park, W.S. Ahn, Synthesis of nanoporous
438   materials via recycling coal fly ash and other solid wastes: A mini review, Chem. Eng. J.
439   317 (2017) 821–843. https://doi.org/10.1016/j.cej.2017.02.124.

440   [5]   M. Sayehi, H. Tounsi, G. Garbarino, P. Riani, G. Busca, Reutilization of silicon- and
441   aluminum- containing wastes in the perspective of the preparation of SiO2-Al2O3 based
442   porous materials for adsorbents and catalysts, Waste Manag. 103 (2020) 146–158.
443   https://doi.org/10.1016/j.wasman.2019.12.013.

444   [6]   W. Cai, J. Yu, C. Anand, A. Vinu, M. Jaroniec, Facile synthesis of ordered mesoporous
445   alumina and alumina-supported metal oxides with tailored adsorption and framework
446   properties, Chem. Mater. 23 (2011) 1147–1157. https://doi.org/10.1021/cm102512v.

447   [7]   C.T. Kresge, M.E. Leonowicz, W.J. Roth, J.C. Vartuli, J.S. Beck, Ordered mesoporous
448   molecular sieves synthesized by a liquid-crystal template mechanism, Nature. 359 (1992)
449   710–712. https://doi.org/10.1038/359710a0.

450   [8]   D. Zhao, J. Feng, Q. Huo, N. Melosh, G. Fredrickson, B. Chmelka, G. Stucky, Triblock
451   Copolymer Syntheses of Mesoporous Silica with Periodic 50 to 300 Angstrom Pores,
452   Science (80-.). 279 (1998) 548–552. https://doi.org/10.1126/science.279.5350.548.

453   [9]   M. Sui, L. She, Review on research and application of mesoporous transitional metal oxides
454   in water treatment, Front. Environ. Sci. Eng. 7 (2013) 795–802.
455   https://doi.org/10.1007/s11783-013-0521-4.

456   [10] Y. Boyjoo, M. Wang, V.K. Pareek, J. Liu, M. Jaroniec, Synthesis and applications of porous
457   non-silica metal oxide submicrospheres, Chem. Soc. Rev. 45 (2016) 6013–6047.
458   https://doi.org/10.1039/c6cs00060f.

459   [11] X. Jiang, N. Suzuki, B.P. Bastakoti, K.C.W. Wu, Y. Yamauchi, Synthesis of continuous
460   mesoporous alumina films with large-sized cage-type mesopores by using diblock
461   copolymers, Chem. - An Asian J. 7 (2012) 1713–1718.
462   https://doi.org/10.1002/asia.201200256.

463   [12] A. Walcarius, C. Delacôte, Rate of Access to the Binding Sites in Organically Modified
464   Silicates. 3. Effect of Structure and Density of Functional Groups in Mesoporous Solids
465   Obtained by the Co-Condensation Route, Chem. Mater. 15 (2003) 4181–4192.
466   https://doi.org/10.1021/cm031089l.

467   [13] V. Hiremath, A.H. Jadhav, H. Lee, S. Kwon, J.G. Seo, Highly reversible CO2 capture using

amino acid functionalized ionic liquids immobilized on mesoporous silica, Chem. Eng. J. 287 (2016) 602–617. https://doi.org/10.1016/j.cej.2015.11.075.

[14] Z.A. Alothman, A review: Fundamental aspects of silicate mesoporous materials, Materials (Basel). 5 (2012) 2874–2902. https://doi.org/10.3390/ma5122874.

[15] B.G. Trewyn, I.I. Slowing, S. Giri, H.T. Chen, V.S.Y. Lin, Synthesis and functionalization of a mesoporous silica nanoparticle based on the sol-gel process and applications in controlled release, Acc. Chem. Res. 40 (2007) 846–853. https://doi.org/10.1021/ar600032u.

[16] B. Yahyaei, S. Azizian, Rapid adsorption of anionic dyes by ordered nanoporous alumina, Chem. Eng. J. 209 (2012) 589–596. https://doi.org/10.1016/j.cej.2012.08.055.

[17] W. Cai, Y. Hu, J. Chen, G. Zhang, T. Xia, Synthesis of nanorod-like mesoporous γ-Al2O3 with enhanced affinity towards Congo red removal: Effects of anions and structure-directing agents, CrystEngComm. 14 (2012) 972–977. https://doi.org/10.1039/C1CE05975K.

[18] B. Yahyaei, S. Azizian, Rapid adsorption of binary dye pollutants onto the nanostructred mesoporous alumina, J. Mol. Liq. 199 (2014) 88–95. https://doi.org/10.1016/j.molliq.2014.08.023.

[19] N.B. Singh, G. Nagpal, S. Agrawal, Rachna, Water purification by using Adsorbents: A Review, Environ. Technol. Innov. 11 (2018) 187–240. https://doi.org/10.1016/j.eti.2018.05.006.

[20] S. Banerjee, Alumina Nanoparticles and Alumina-Based Adsorbents for Wastewater Treatment, Elsevier Inc., 2016. https://doi.org/10.1016/b978-0-12-804609-8.00010-8.

[21] M.M. Ibrahim, Cr2O3/Al2O3 as adsorbent: Physicochemical properties and adsorption behaviors towards removal of Congo red dye from water, J. Environ. Chem. Eng. 7 (2019) 102848. https://doi.org/10.1016/j.jece.2018.102848.

[22] J. Ge, K. Deng, W. Cai, J. Yu, X. Liu, J. Zhou, Effect of structure-directing agents on facile hydrothermal preparation of hierarchical γ-Al2O3 and their adsorption performance toward Cr(VI) and CO2, J. Colloid Interface Sci. 401 (2013) 34–39. https://doi.org/10.1016/j.jcis.2013.03.028.

[23] W. Li, C.Y. Cao, L.Y. Wu, M.F. Ge, W.G. Song, Superb fluoride and arsenic removal performance of highly ordered mesoporous aluminas, J. Hazard. Mater. 198 (2011) 143–150. https://doi.org/10.1016/j.jhazmat.2011.10.025.

[24] C. Han, H. Li, H. Pu, H. Yu, L. Deng, S. Huang, Y. Luo, Synthesis and characterization of

499   mesoporous alumina and their performances for removing arsenic(V), Chem. Eng. J. 217

500   (2013) 1–9. https://doi.org/10.1016/j.cej.2012.11.087.

501 [25] M.E. Mahmoud, O.F. Hafez, M.M. Osman, A.A. Yakout, A. Alrefaay, Hybrid

502   inorganic/organic alumina adsorbents-functionalized-purpurogallin for removal and

503   preconcentration of Cr(III), Fe(III), Cu(II), Cd(II) and Pb(II) from underground water, J.

504   Hazard. Mater. 176 (2010) 906–912. https://doi.org/10.1016/j.jhazmat.2009.11.122.

505 [26] S. Verenich, A. Laari, M. Nissen, J. Kallas, Combination of coagulation and catalytic wet

506   oxidation for the treatment of pulp and paper mill effluents, Water Sci. Technol. 44 (2001)

507   145–152. https://doi.org/10.2166/wst.2001.0273.

508 [27] M. Saeli, L. Senff, D.M. Tobaldi, G. La Scalia, M.P. Seabra, J.A. Labrincha, Innovative

509   recycling of lime slaker grits from paper-pulp industry reused as aggregate in ambient cured

510   biomass fly ash-based geopolymers for sustainable construction material, Sustain. 11 (2019)

511   1–15. https://doi.org/10.3390/su11123481.

512 [28] D. Bojinova, R. Teodosieva, Leaching of valuable elements from thermal power plant bottom

513   ash using a thermo-hydrometallurgical process, Waste Manag. Res. 34 (2016) 511–517.

514   https://doi.org/10.1177/0734242X16633775.

515 [29] K. Yin, A. Ahamed, G. Lisak, Environmental perspectives of recycling various combustion

516   ashes in cement production – A review, Waste Manag. 78 (2018) 401–416.

517   https://doi.org/10.1016/j.wasman.2018.06.012.

518 [30] M.J. Quina, E. Bontempi, A. Bogush, S. Schlumberger, G. Weibel, R. Braga, V. Funari, J.

519   Hyks, E. Rasmussen, J. Lederer, Technologies for the management of MSW incineration

520   ashes from gas cleaning: New perspectives on recovery of secondary raw materials and

521   circular economy, Sci. Total Environ. 635 (2018) 526–542.

522   https://doi.org/10.1016/j.scitotenv.2018.04.150.

523 [31] F. Huber, H. Herzel, C. Adam, O. Mallow, D. Blasenbauer, J. Fellner, Combined disc

524   pelletisation and thermal treatment of MSWI fly ash, Waste Manag. 73 (2018) 381–391.

525   https://doi.org/10.1016/j.wasman.2017.12.020.

526 [32] F.C. Silva, N.C. Cruz, L.A.C. Tarelho, S.M. Rodrigues, Use of biomass ash-based materials

527   as soil fertilisers: Critical review of the existing regulatory framework, J. Clean. Prod. 214

528   (2019) 112–124. https://doi.org/10.1016/j.jclepro.2018.12.268.

529 [33] L. Reijnders, Disposal, uses and treatments of combustion ashes: A review, Resour. Conserv.

530   Recycl. 43 (2005) 313–336. https://doi.org/10.1016/j.resconrec.2004.06.007.

531 [34] J. Pizarro, X. Castillo, S. Jara, C. Ortiz, P. Navarro, H. Cid, H. Rioseco, D. Barros, N. Belzile,
532   Adsorption of Cu2+ on coal fly ash modified with functionalized mesoporous silica, Fuel.
533   156 (2015) 96–102. https://doi.org/10.1016/j.fuel.2015.04.030.

534 [35] K. Chojnacka, I. Michalak, Using wood and bone ash to remove metal ions from solutions,
535   Glob. Nest J. 11 (2009) 205–217. https://doi.org/10.30955/gnj.000582.

536 [36] M. Gómez, J. Pizarro, X. Castillo, A. Ghisolfi, C. Díaz, M. de Lourdes Chávez, D. Cazorla-
537   Amorós, Development of mesoporous materials from biomass ash with future applications
538   as   adsorbent   materials,   Microporous   Mesoporous   Mater.   299   (2020).
539   https://doi.org/10.1016/j.micromeso.2020.110085.

540 [37] S. Chaturvedi, P.N. Dave, Removal of iron for safe drinking water, Desalination. 303 (2012)
541   1–11. https://doi.org/10.1016/j.desal.2012.07.003.

542 [38] W.S.W. Ngah, S. Ab Ghani, A. Kamari, Adsorption behaviour of Fe(II) and Fe(III) ions in
543   aqueous solution on chitosan and cross-linked chitosan beads, Bioresour. Technol. 96 (2005)
544   443–450. https://doi.org/10.1016/j.biortech.2004.05.022.

545 [39] Y. Guo, Y. Li, F. Cheng, M. Wang, X. Wang, Role of additives in improved thermal
546   activation of coal fly ash for alumina extraction, Fuel Process. Technol. 110 (2013) 114–
547   121. https://doi.org/10.1016/j.fuproc.2012.12.003.

548 [40] W. Cai, L. Tan, J. Yu, M. Jaroniec, X. Liu, B. Cheng, F. Verpoort, Synthesis of amino-
549   functionalized mesoporous alumina with enhanced affinity towards Cr(VI) and CO2, Chem.
550   Eng. J. 239 (2014) 207–215. https://doi.org/10.1016/j.cej.2013.11.011.

551 [41] K.S.W. Sing, Reporting physisorption data for gas/solid systems with special reference to the
552   determination of surface area and porosity (Provisional), Pure Appl. Chem. 54 (1982) 2201–
553   2218. https://doi.org/10.1351/pac198254112201.

554 [42] Y. Yang, Y. Xu, B. Han, B. Xu, X. Liu, Z. Yan, Effects of synthetic conditions on the textural
555   structure   of   pseudo-boehmite,   J.   Colloid   Interface   Sci.   469   (2016)   1–7.
556   https://doi.org/10.1016/j.jcis.2016.01.053.

557 [43] M. Liu, H. Yang, Facile synthesis and characterization of macro-mesoporous γ-Al2O3,
558   Colloids   Surfaces   A   Physicochem.   Eng.   Asp.   371   (2010)   126–130.
559   https://doi.org/10.1016/j.colsurfa.2010.09.022.

560 [44] M. Benítez Guerrero, L.A. Pérez-Maqueda, P.P. Castro, J. Pascual Cosp, Alúminas porosas:

El método de bio-réplica para la síntesis de alúminas estables de alta superficie específica, Bol. La Soc. Esp. Ceram. y Vidr. 52 (2013) 251–267. https://doi.org/10.3989/cyv.322013.

[45] C. Morterra, C. Emanuel, G. Cerrato, G. Magnacca, Infrared study of some surface properties of boehmite (γ-AlO2H), J. Chem. Soc. Faraday Trans. 88 (1992) 339–348. https://doi.org/10.1039/FT9928800339.

[46] G. Wanka, H. Hoffmann, W. Ulbricht, Phase Diagrams and Aggregation Behavior of Poly(oxyethylene)-Poly(oxypropylene)-Poly(oxyethylene) Triblock Copolymers in Aqueous Solutions, Macromolecules. 27 (1994) 4145–4159. https://doi.org/10.1021/ma00093a016.

[47] F. Liu, X. Zheng, J. Chen, Y. Zheng, L. Jiang, Controlling the synthesis and application of nanocrystalline spherical and ordered mesoporous alumina with high thermal stability, RSC Adv. 5 (2015) 93917–93925. https://doi.org/10.1039/c5ra12111f.

[48] W. Wu, Z. Wan, M. Zhu, D. Zhang, A facile route to aqueous phase synthesis of mesoporous alumina with controllable structural properties, Microporous Mesoporous Mater. 223 (2016) 203–212. https://doi.org/10.1016/j.micromeso.2015.11.004.

[49] G. Barraza-Garza, L.A. De La Rosa, A. Martínez-Martínez, H. Castillo-Michel, M. Cotte, E. Alvarez-Parrilla, La microespectroscopía de infrarrojo con transformada de fourier (FTIRM) en el estudio de sistemas biológicos, Rev. Latinoam. Quim. 41 (2013) 125–148. http://www.scielo.org.mx/scielo.php?script=sci_arttext&pid=S0370-59432013000300001&lng=es&tlng=es.

[50] F.C. Liu, P. Dong, W. Lu, K. Sun, On formation of Al–O–C bonds at aluminum/polyamide joint interface, Appl. Surf. Sci. 466 (2019) 202–209. https://doi.org/10.1016/j.apsusc.2018.10.024.

[51] M. Meng, L. Stievano, J.F. Lambert, Adsorption and thermal condensation mechanisms of amino acids on oxide supports. 1. Glycine on silica, Langmuir. 20 (2004) 914–923. https://doi.org/10.1021/la035336b.

[52] B.M. Messer, C.D. Cappa, J.D. Smith, K.R. Wilson, M.K. Gilles, R.C. Cohen, R.J. Saykally, pH dependence of the electronic structure of glycine, J. Phys. Chem. B. 109 (2005) 5375–5382. https://doi.org/10.1021/jp0457592.

[53] S. Prabhu, K. Cheirmadurai, J. Raghava Rao, P. Thanikaivelan, Glycine functionalized alumina nanoparticles stabilize collagen in ethanol medium, Bull. Mater. Sci. 39 (2016)

592   223–228. https://doi.org/10.1007/s12034-015-1126-2.

593 [54] D. Briggs, X-ray photoelectron spectroscopy (XPS), Handb. Adhes. Second Ed. (2005) 621–
594   622. https://doi.org/10.1002/0470014229.ch22.

595 [55] L. Zhang, A. Chatterjee, K.T. Leung, Three-stage growth of glycine and glycylglycine
596   nanofilms on Si(111)7×7 and their thermal evolution in ultrahigh vacuum condition: From
597   chemisorbed adstructures to transitional adlayer to zwitterionic films, J. Phys. Chem. C. 115
598   (2011) 14155–14163. https://doi.org/10.1021/jp110055d.

599 [56] P. Maneechakr, S. Karnjanakom, Adsorption behaviour of Fe(II) and Cr(VI) on activated
600   carbon: Surface chemistry, isotherm, kinetic and thermodynamic studies, J. Chem.
601   Thermodyn. 106 (2017) 104–112. https://doi.org/10.1016/j.jct.2016.11.021.

602 [57] T. Bakalár, M. Kanuchová, A. Girová, H. Pavolová, R. Hromada, Z. and Hajduová,
603   Characterization of Fe (III) Adsorption onto Zeolite and Bentonite, Int. J. Environ. Res.
604   Public Heal. 17 (2020) 5718. https://doi.org/10.3390/ijerph17165718.

605 [58] W. Konicki, M. Aleksandrzak, E. Mijowska, Equilibrium and kinetics studies for the
606   adsorption of Ni2+ and Fe3+ ions from aqueous solution by graphene oxide, Polish J. Chem.
607   Technol. 19 (2017) 120–129. https://doi.org/10.1515/pjct-2017-0058.

608 [59] B. Schmidt, J. Rokicka, J. Janik, K. Wilpiszewska, Preparation and characterization of potato
609   starch copolymers with a high natural polymer content for the removal of cu(II) and fe(III)
610   from solutions, Polymers (Basel). 12 (2020) 1–22. https://doi.org/10.3390/polym12112562.

611 [60] S.B. Khan, M.M. Rahman, H.M. Marwani, A.M. Asiri, K.A. Alamry, M.A. Rub, Selective
612   adsorption and determination of iron(III): Mn3O4/TiO2 composite nanosheets as marker of
613   iron for environmental applications, Appl. Surf. Sci. 282 (2013) 46–51.
614   https://doi.org/10.1016/j.apsusc.2013.03.180.

615 [61] S. Parambadath, A. Mathew, S.Y. Kim, S.S. Park, C.S. Ha, Fe3+-bis-ethylenediamine
616   complex bridged periodic mesoporous organosilica for the efficient removal of arsenate and
617   chromate, Pure Appl. Chem. 90 (2018) 869–884. https://doi.org/10.1515/pac-2017-0909.

618 [62] K. Barquist, S.C. Larsen, Chromate adsorption on bifunctional, magnetic zeolite composites,
619   Microporous Mesoporous Mater. 130 (2010) 197–202.
620   https://doi.org/10.1016/j.micromeso.2009.11.005.

621 [63] S. He, Y. Li, L. Weng, J. Wang, J. He, Y. Liu, K. Zhang, Q. Wu, Y. Zhang, Z. Zhang,
622   Competitive adsorption of Cd2+, Pb2+ and Ni2+ onto Fe3+-modified argillaceous

limestone: Influence of pH, ionic strength and natural organic matters, Sci. Total Environ. 637–638 (2018) 69–78. https://doi.org/10.1016/j.scitotenv.2018.04.300.

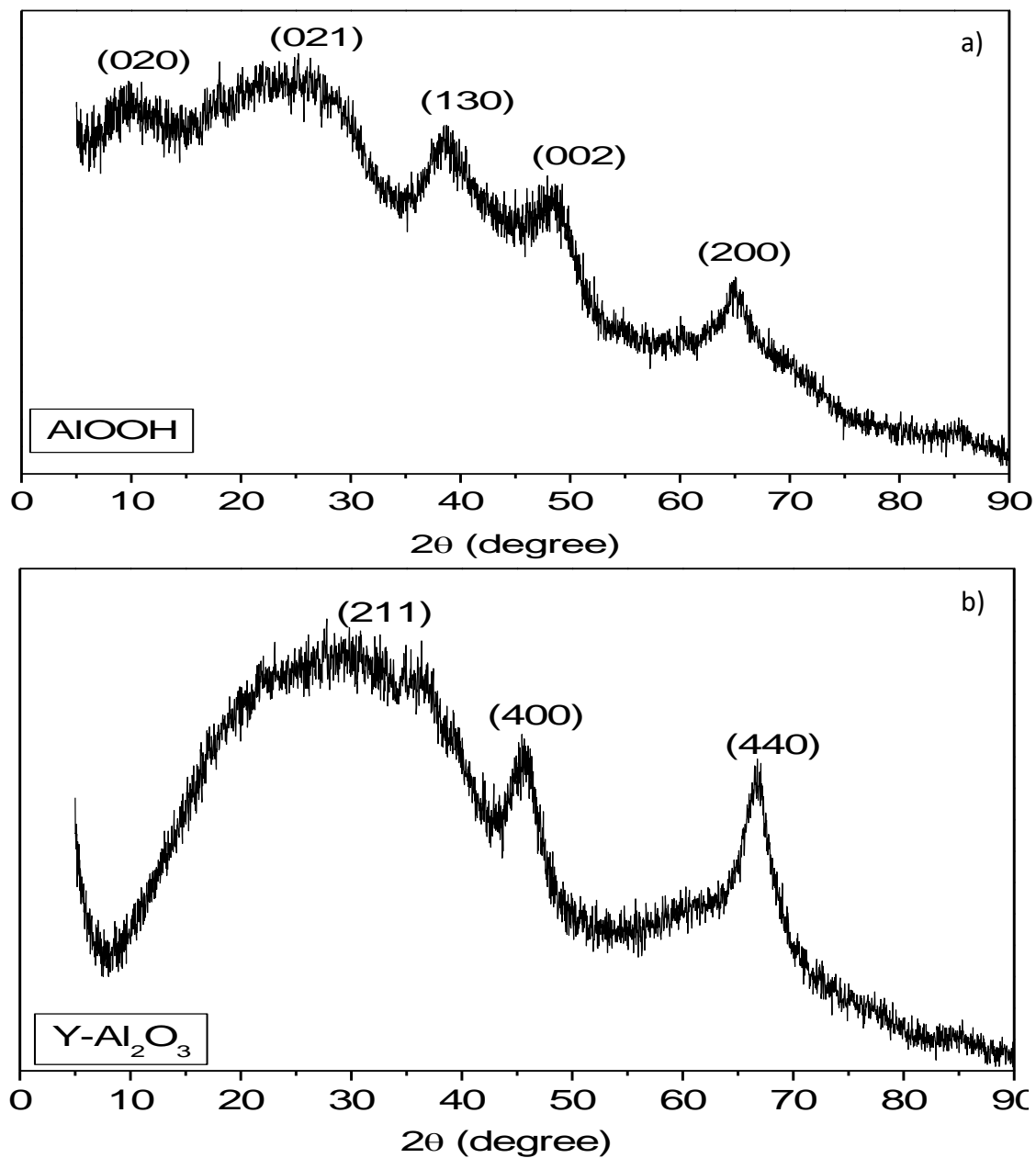[64] M.J. Eckelman, J.B. Zimmerman, P.T. Anastas, Toward green nano: E-factor analysis of several nanomaterial syntheses, J. Ind. Ecol. 12 (2008) 316–328. https://doi.org/10.1111/j.1530-9290.2008.00043.x.

630 **Figures captions**

631

Fig. 1. XRD pattern a) AlOOH extracted from CBT. b) γ-Al_2O_3 before the synthesize with Pluronic P-123

635
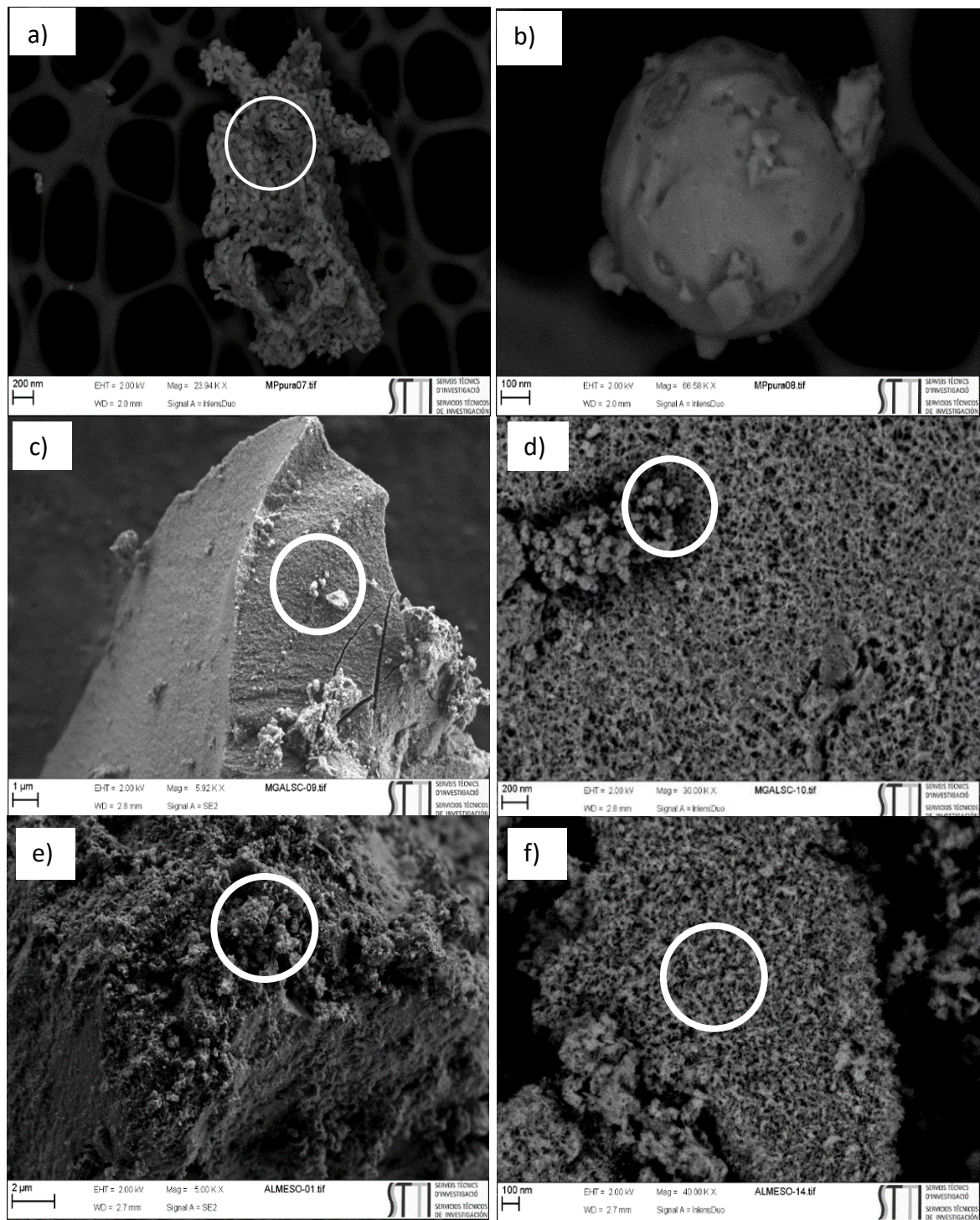
Fig. 2. FE-SEM micrographs of CTB a) lower and b) higher magnifications; AlOOH, c) lower and d) higher magnifications and γ-Al$_2$O$_3$, e) lower and f) higher magnifications. The samples have been marked with white circles to highlight the differences between the samples, facilitating their analysis

641
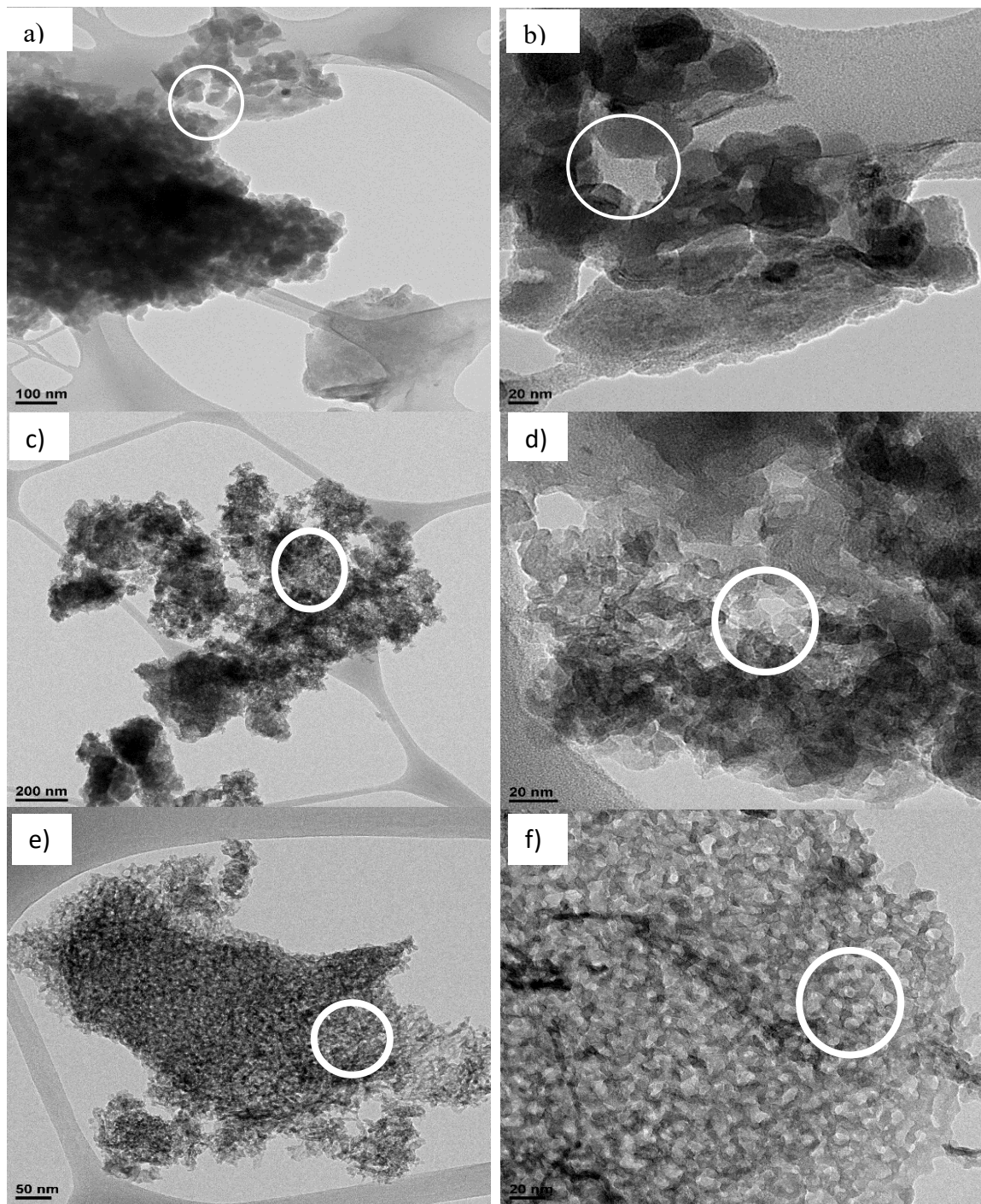
Fig. 3. TEM micrographs of CBT, a) lower and b) higher magnifications; AlOOH

c) lower and d) higher magnifications and γ-Al$_2$O$_3$, e) lower and f) higher

magnifications. The samples have been marked with white circles to highlight the

differences between the samples, facilitating their analysis
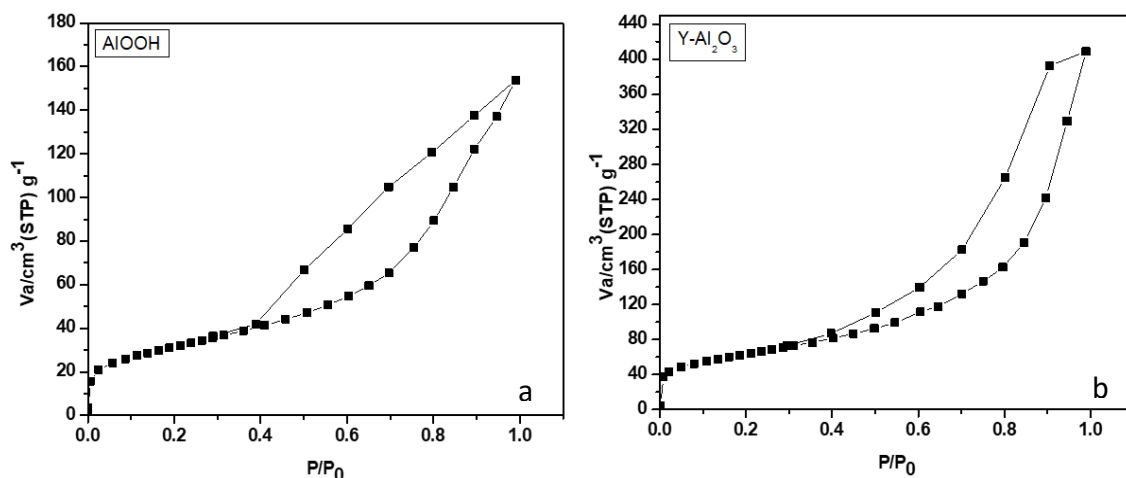
647

648　**Fig. 4.** N_2 at 77 K adsorption-desorption isotherm a) AlOOH. b) γ-Al_2O_3

649

650
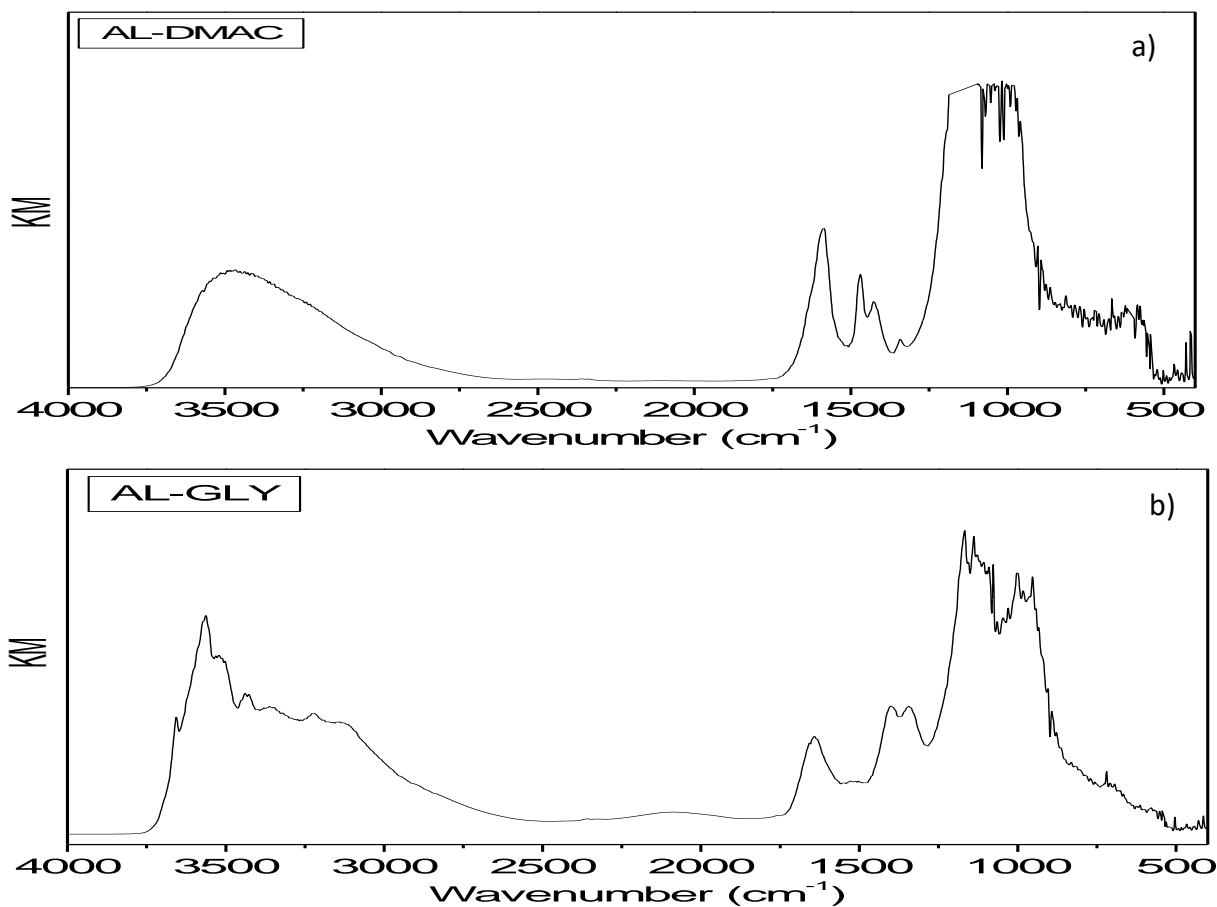
651

652　**Fig. 5.** a) DRIFT spectrum and schemes of γ-Al_2O_3 before the functionalization with N,N-

653　　dimethylacetamide (Al-DMAC). b) DRIFT spectrum and schemes of γ-Al_2O_3 before

654   the functionalization with glycine (Al-GLY)

655

656
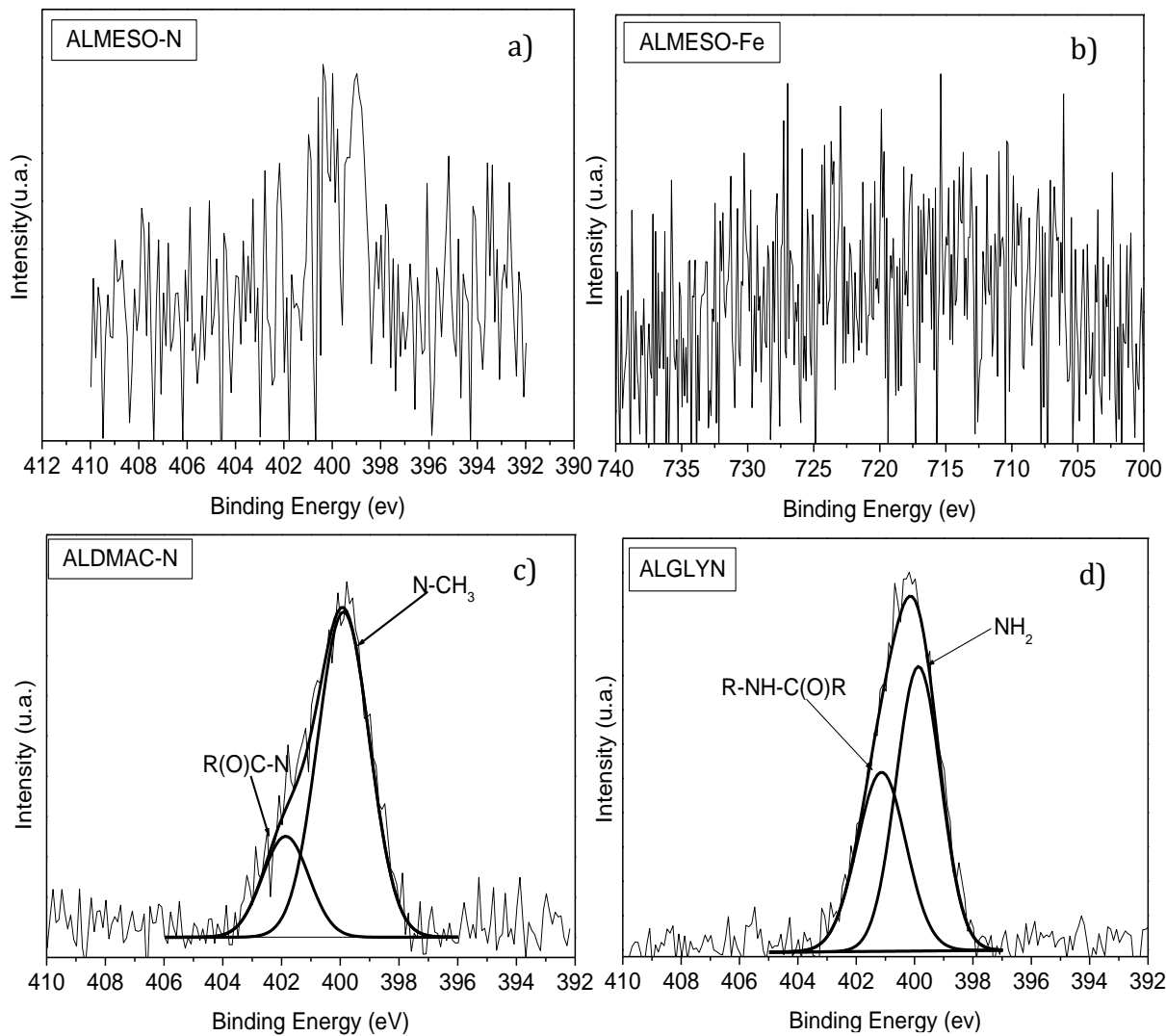
Fig. 6. XPS high resolution spectra for a) N 1s and b) Fe 2p of γ-Al_2O_3. c) N 1s of Al-DMAC.

658   d) N 1s of Al-GLY

659

660
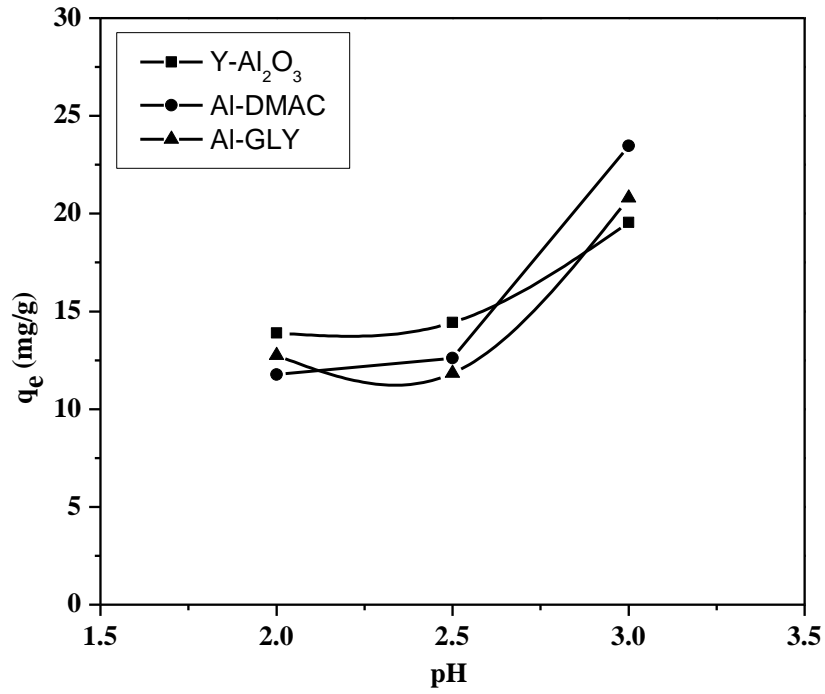
Fig. 7. Effect of pH on the adsorption of Fe^{3+} on 0.01 g of γ-Al_2O_3, Al-DMAC and Al-GLY

from 5 mL of 50 mg L^{-1} $Fe(NO_3)_3$ solution and 30 min of constant stirring (200 rpm)

663

664
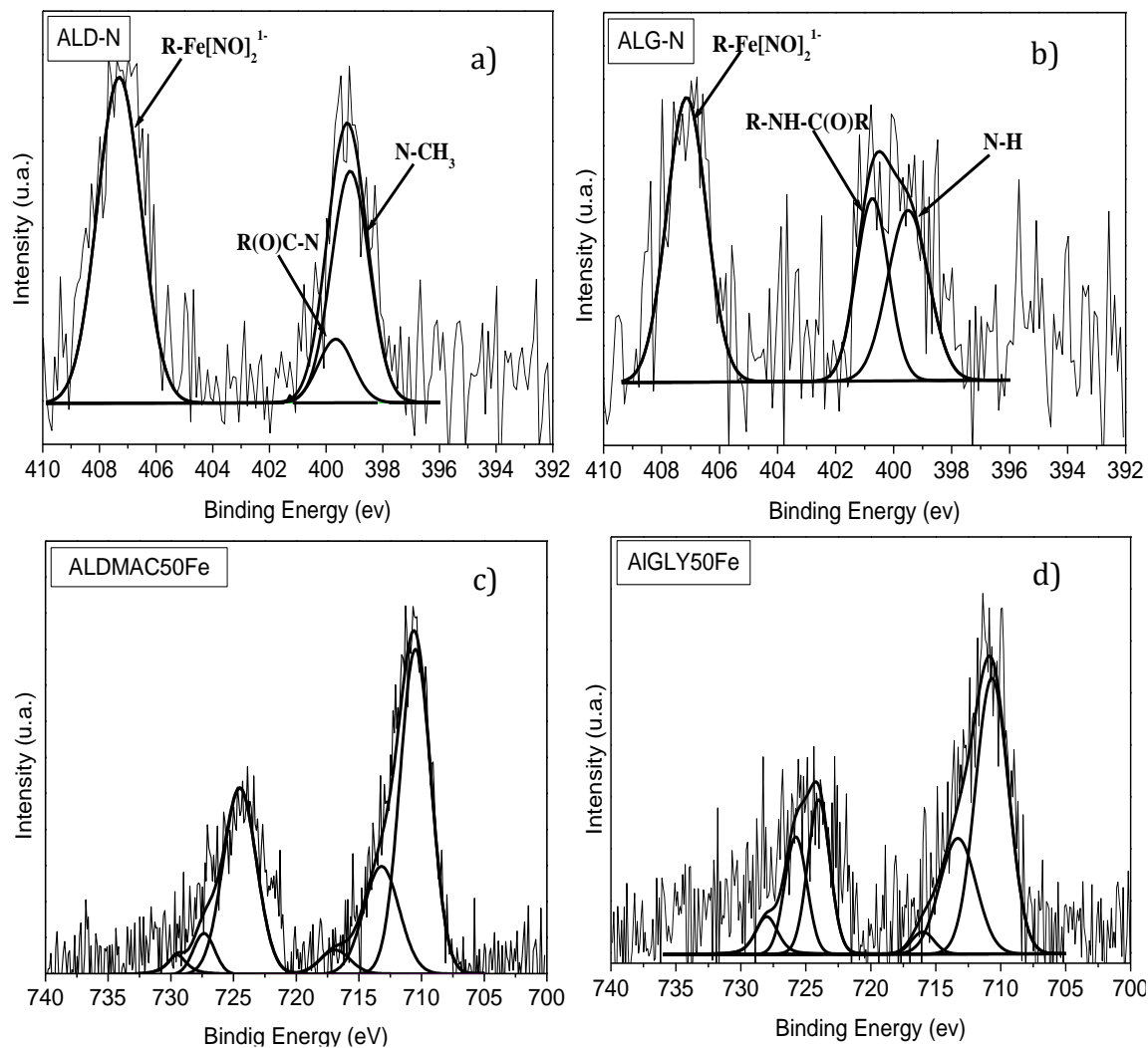
Fig. 8. XPS high resolution spectra before adsorption of Fe^{3+} a) N 1s and c) Fe 2p of Al-
DMAC. b) N 1s and d) Fe 2p of Al-GLY. The adsorption of Fe^{3+} on 0.01 g of Y-
Al_2O_3, Al-DMAC and Al-GLY from 5 mL of 50 mg L^{-1} $Fe(NO_3)_3$ solution and 30
min of constant stirring (200 rpm)

671   **Table 1** Present elements wt. % at CBT obtained by X-ray Fluorescence (XRF).

Phases	SiO_2	Al_2O_3	Fe_2O_3	CaO	P_XC	MgO	Na_2O	P_2O_5	TiO_2	MnO
CBT	47.2	19.5	9.3	8.1	3.9	3.9	2.4	2.1	1.2	0.7

Elements	O	F	Al	Si	Cl	S	P	Fe	Cu	V
AlOOH	41.2	5.3	43.2	0.8	7.8	1.0	0.1	0.2	0.1	0.2
γ-Al_2O_3	47.0	0.9	49.3	0.9	0.5	1.0	0.2	0.1	0.1	0.2

672

673

674

675

676   **Table 2** Porous texture data obtained by adsorption-desorption isotherm of N_2 at 77 K

677   (surface area by BET method, total pore volume and average pore size determined

678   by BJH method) for CBT and AlOOH and γ-Al_2O_3 obtained in this work and

679   compared to the mesoporous γ-Al_2O_3 obtained by Cai et al. [22].

	SBET (m^2 g^{-1})	Vp BJH (cm^3 g^{-1})	Average dp BJH (nm)
CBT	18	0.04	3.8
AlOOH	115	0.25	3.6
γ-Al_2O_3	230	0.51	8.9
γ-Al_2O_3 by Cai et al.	24	0.07	10.9

680

681

682

683

684   **Table 3** Fe^{3+} removal capacity in q_e (mg q^{-1}) and percentage by synthesised matrices.

pH	Y-Al_2O_3		Al-DMAC		Al-GLY	
	q_e (mg g^{-1})	(% Ads.)	q_e (mg g^{-1})	(% Ads.)	q_e (mg g^{-1})	(% Ads.)
2.0	13.90	51.61	11.76	47.05	12.74	50.59
2.5	14.44	57.77	12.61	50.45	11.83	47.34
3.0	19.55	78.20	23.47	93.88	20.80	83.21

685

686

687

688 **Table 4** Adsorption efficiencies (AE) of Fe(III) to pH 3 for various adsorbents with maximum

689 AE.

Adsorbent	Surface functional group	AE mg g-1	Initial pH	Reference
Y-Al$_2$O$_3$	-OH	19.55	3.0	This paper
Al-DMAC	-OH, -N-C	23.47	3.0	This paper
Al-GLY	-OH, -NH$_2$	20.80	3.0	This paper
Activated Carbon (agro-residue)	-OH, -COOH	21.69	2.7	56
Bentonite—BR	-OH	16.86	-------	57
Zeolite—M20	-OH	10.19	--------	57
Graphene Oxide	-OH, -COOH	21.9	4.0	58
Starch-g-polyacrylamide	-OH, -NH, -C=O	21.20	------	59
Mn$_3$O$_4$/TiO$_2$ composite nanosheets	M-O	< 20.00	5.0	60

690

691